ACS Photonics

Letter

Cite This: ACS Photonics 2018, 5, 759−764

meV Resolution in Laser-Assisted Energy-Filtered Transmission Electron Microscopy

Enrico Pomarico,[†] Ivan Madan,[†] Gabriele Berruto,[†] Giovanni Maria Vanacore,[†] Kangpeng Wang,[‡] Ido Kaminer,[‡] F. Javier García de Abajo,[§,∥] and Fabrizio Carbone*[,†]

[†]Laboratory for Ultrafast Microscopy and Electron Scattering (LUMES), Institute of Physics, École Polytechnique Fédérale de Lausanne (EPFL), Lausanne CH-1015, Switzerland

[‡]Andrew and Erna Viterbi Department of Electrical Engineering, Technion−Israel Institute of Technology, Haifa, Israel

[§]ICFO-Institut de Ciencies Fotoniques, The Barcelona Institute of Science and Technology, 08860 Castelldefels (Barcelona), Spain

[∥]ICREA-Institució Catalana de Recerca i Estudis Avançats, Passeig Lluís Companys, 23, 08010 Barcelona, Spain

Supporting Information

ABSTRACT: The electronic, optical, and magnetic properties of quantum solids are determined by their low-energy (<100 meV) many-body excitations. Dynamical characterization and manipulation of such excitations rely on tools that combine nm-spatial, fs-temporal, and meV-spectral resolution. Currently, phonons and collective plasmon resonances can be imaged in nanostructures with atomic (sub-nm) and tens of meV space/energy resolution using state-of-the-art energy-filtered transmission electron microscopy (TEM), but only under static conditions, while fs-resolved measurements are common but lack spatial or energy resolution. Here, we demonstrate a new method of spectrally resolved photon-induced near-field electron microscopy (SRPINEM) that allows us to obtain nm-fs-resolved maps of nanoparticle plasmons with an energy resolution determined by the laser line width (20 meV in this work) and no longer limited by the electron beam and spectrometer energy spreading. This technique can be extended to any optically accessible low-energy mode, thus pushing TEM to a previously unattainable spectral domain with an unprecedented combination of space, energy, and temporal resolution.

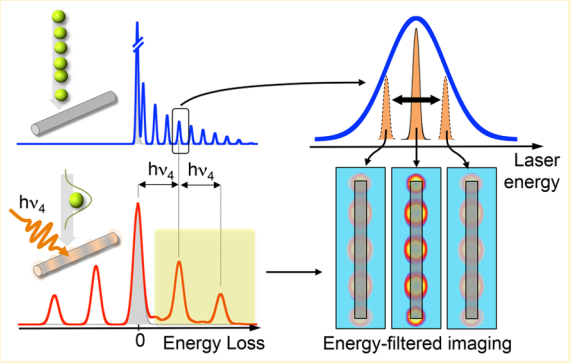

KEYWORDS: *ultrafast transmission electron microscopy, photon-induced near-field microscopy, electron energy-loss spectroscopy, high-resolution microscopy, plasmonics, surface-plasmon polaritons*

In solids, low-energy many-body states emerge from the complex interplay between topology, electronic correlations, and structural dynamics.[1] Electron- and photon-based inelastic scattering techniques can access this realm to provide information on energy scales and dispersion relations via spectroscopy[2] and on symmetry via selection rules.[3] When combined with microscopy, such as in energy-filtered electron microscopes, sub-nm spatial resolution can also be reached.[4] However, the energy resolution of these methods is fundamentally limited by the energy spread of the probe beam, which forbids access to features in the far-infrared spectral region. This limitation is further incremented by the finite energy resolution of the spectrometer.[5] For these reasons, much effort is currently under way to develop tools with improved energy resolution, simultaneously combined with space and time resolution, capable of resolving the structural, electronic, and magnetic textures that characterize quantum solids and nanostructures.

A way to circumvent the energy-resolution problem is offered by laser-based pump−probe methods, in which low-energy modes correspond to long-period oscillations that can be coherently excited by light pulses and directly probed in real time via spectroscopy[6,7] or microscopy.[8,9] Time-resolved methods further enable the actual determination of the lifetimes of specific excitations,[10] avoiding indirect estimates based upon static spectroscopic data.[11] Additionally, time-resolved methods offer a unique handle to control the out-of-equilibrium properties of a solid.[12] Unfortunately, all-optical pump−probe techniques are limited by diffraction in far-field microscopes and by interaction with a sampling tip in near-field setups, yielding a spatial resolution of tens of nm at best.[13,14]

Recently, pulsed electron beams have been combined with ultrafast lasers to simultaneously achieve nm-fs space−time resolution in the technique known as photon-induced near-field electron microscopy (PINEM),[15−19] successfully applied in selecting specific plasmonic excitations, without resorting to complex electron-wave function shaping techniques,[20] as well as in mapping their dynamics at surfaces,[9] interfaces,[21] and

Received: November 19, 2017
Published: December 21, 2017

DOI: 10.1021/acsphotonics.7b01393
ACS Photonics 2018, 5, 759−764

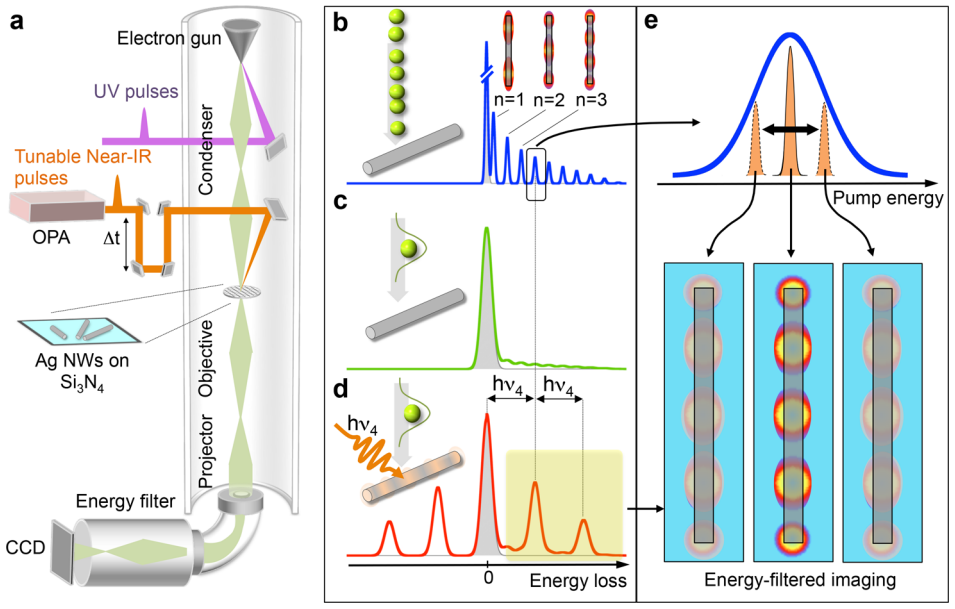

Figure 1. Spectrally resolved photon-induced near-field electron microscopy: experimental setup and concept. (a) Scheme of the experimental apparatus. (b) EELS spectrum revealing multiple plasmon resonances in an individual nanowire, excited by the passing electrons and mapped with nm resolution by raster scanning the electron beam (plasmon map insets). (c) Sketch of an EELS spectrum of the nanowire under ultrafast energy-filtered microscopy conditions. The visibility of the electron-induced plasmon resonances is severely reduced. (d) Sketch of an EELS spectrum of the nanowire upon photoexcitation by light pulses of energy $h\nu_4$, tuned to the $n = 4$ plasmon-resonance frequency. This specific mode exchanges several times its characteristic energy with the electrons. (e) Concept of our experiment: the laser excitation wavelength is scanned and the plasmon resonance profile retrieved via quantitative analysis of the energy-filtered images.

buried layers.[22] However, energy resolution in PINEM is obtained through an electron spectrometer, so the results are also affected by energy spread in the electron beam, which in practice limits the resolution to the eV range. Better energy resolution of ∼10 meV has been recently reported in state-of-the-art TEMs through electron energy-loss spectroscopy (EELS),[23−25] but with much poorer or no time resolution. The sought-after nm-fs-meV combined resolution is therefore remaining as an insurmountable challenge with currently existing approaches.

To go beyond these limitations, we have developed a disruptive approach that adopts tunable-wavelength light pulses from an optical parametric amplifier (OPA) for photoexcitation combined with energy-filtered transmission electron microscopy (TEM) (Figure 1, see details in Methods). A scheme of our experimental apparatus is depicted in Figure 1a. We demonstrate the potential of our technique by applying it to study plasmon resonances (PRs) in long metal nanowires (NWs), driven by the strong potential of these excitations in a broad range of areas including optical sensing[26] and, more recently, optoelectronics at infrared energies in 2D materials.[27,14] The study of plasmons has a long tradition in electron microscopy[23,28] and should benefit from combined nm-fs-meV resolution.

In general, the transient electric field associated with the passage of swift electrons in the proximity of a nanostructure excites PRs, which are visible as features in an energy-loss spectrum (Figure 1b). In time-resolved electron microscopy, the intensity of the electron pulses is severely attenuated to reduce space charge effects[29] and their energy bandwidth is broadened at the eV level, thus resulting in significantly reduced contrast of the plasmon features (Figure 1c). In contrast, in PINEM, a specific plasmon resonance can be strongly excited by illuminating the nanostructure with laser pulses at a resonant energy, resulting in the exchange of multiples of the PR energy with the imaging electron beam (Figure 1d): the external laser supplies photons in a coherent state, which consequently populate the plasmon also in a coherent state with average occupancy $n_o \gg 1$ for high light intensities; multiple plasmon gains and losses by the electron then take place with a probability proportional to n_o times the spectral probability in conventional EELS.[30] For this reason, in PINEM, filtering the electron beam to image all inelastically scattered electrons yields the spatial profile of one specific PR, unlike conventional spectral imaging, which requires a filtering pass-energy tuned to the individual resonance. Ultimately, by scanning the laser wavelength across PRs and mapping their spatial profile in real space via PINEM imaging, one can resolve the modes with an energy resolution given by the laser line width (Figure 1e) and thus no longer limited by the electron-beam energy bandwidth.

In our spectrally resolved PINEM (SRPINEM) method, we use an electron beam with $\sim 10^2$ electrons per pulse at the specimen position in combination with the photoexciting light pulses. The energy distribution of such a beam is depicted in Figure 2a before and after the arrival of the photoexcitation with 100 fs, 1.08 eV, 5 mJ/cm^2 pulses. The electron-beam energy spread is as large as 6 eV due to intrapulse electron−electron Coulomb repulsion.[29] Importantly, the overall spectrum changes when electrons and light pulses arrive in coincidence at the NW (Figure 2a, red trace). A depletion is observed close to the zero of energy (referenced to the TEM acceleration voltage, 200 kV) corresponding to the zero-loss peak (ZLP) and accompanied by an increase of counts toward the tails of the spectrum. This is a typical fingerprint of the PINEM effect, which originates from inelastic scattering of the electrons by the photoexcited surface-plasmon polaritons (SPPs). Note that, as schematically depicted in Figure 1c,

DOI: 10.1021/acsphotonics.7b01393
ACS Photonics 2018, 5, 759−764

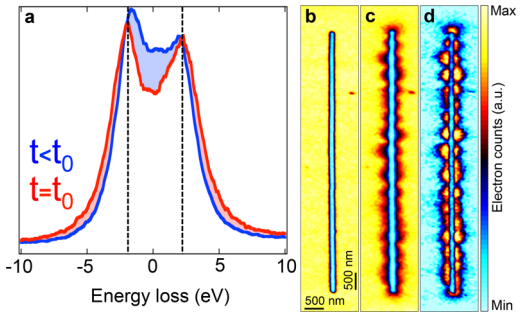

Figure 2. Plasmon imaging method. (a) EELS spectrum of the nanowire taken with ~10^2 electrons per pulse before (blue) and during (red) the light excitation at time t_0. (b, c) Nanowire images with (c) and without (b) light excitation. (d) Plasmon image obtained as the difference between b and c.

the PINEM sidebands are not resolved because of the large energy bandwidth of the electron beam. However, by subtracting an image recorded before illumination (Figure 2b) from one recorded in coincidence with the photoexcitation (Figure 2c), the spatial distribution of the photoinduced plasmonic field is clearly retrieved (Figure 2d). In this specific instance, Figure 2d highlights the resonance mode of order n = 16 (number of near-field nodes along the wire length) in a silver NW (130 nm diameter, 7.8 μm length) deposited on a Si_3N_4 membrane (see Methods).

While this method in principle works for arbitrarily low-energy optically allowed excitations, its limit is given by the sensitivity in detecting the laser-induced depletion of the elastic peak. For very low energy modes (around 10 meV) in the weak coupling limit, yielding only a few PINEM sidebands, the ZLP shape changes may fall below the resolution of the EELS spectrometer (50 meV in our case), thus preventing the laser on/off difference image from showing the spatial profile of the photoexcited mode.

We resolve the spectral line shape of the PRs supported by the silver NW by applying the described method to record a series of images as a function of the photoexciting laser wavelength. When the photon energy is tuned to a PR (Figure 3), a clear spatial profile is obtained, revealing the order of the mode n through the number of PINEM intensity nodes along the wire (Figure 3b). This is also evidenced by the spatial Fourier transform (FT) of the image, which allows us to retrieve the spatial periodicity of the field and the strength of the resonance. By plotting the area of the FT peak associated with a particular PR as a function of the driving laser wavelength, we finally obtain the plasmon spectral profile with an energy resolution of 20 meV, only limited by the laser line width (Figure 3c). As the absolute Fourier limit of the laser pulse cannot be bypassed, a spectral/temporal trade-off is needed. In our current study, the laser system was prepared to deliver tunable near-infrared (near-IR) ~100 fs pulses with ~20 meV bandwidth, adapted to resolve the PR spectral shape and its temporal dynamics. To reach a finer energy resolution (less than 5 meV), one could employ pulses of 1−2 ps duration, sacrificing time resolution, or with longer wavelengths in the mid-IR regime. The latter method could be of interest for example to study long-lived, sharp plasmons, such as those in high-quality graphene.[14]

Notably, our technique allows one to combine nm-fs-meV energy−space−time resolution in a single experiment, yielding a complete characterization of a low-energy collective mode. In Figure 4a, we show our measured spectra of the wire PRs in the range between 800 and 1080 meV (see supplementary

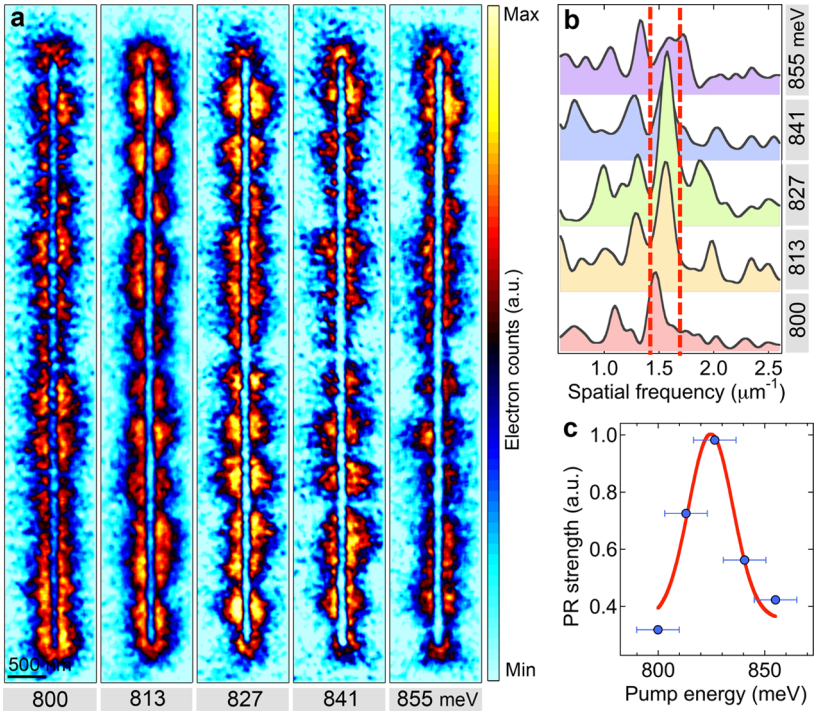

Figure 3. Laser-assisted plasmon spectroscopy. (a) TEM images of the n = 13 plasmon resonance for selected photoexcitation energies around 827 meV (1500 nm, central image). (b) Fourier transform (FT) of the parallel-to-the-wire spatial profile in these images for the different pump energy values. (c) Integral of the pump energy-dependent FT within the region of spatial frequencies corresponding to the mode n = 13 (indicated by red dashed lines in b), fitted with a Gaussian function (red curve).

DOI: 10.1021/acsphotonics.7b01393
ACS Photonics 2018, 5, 759−764

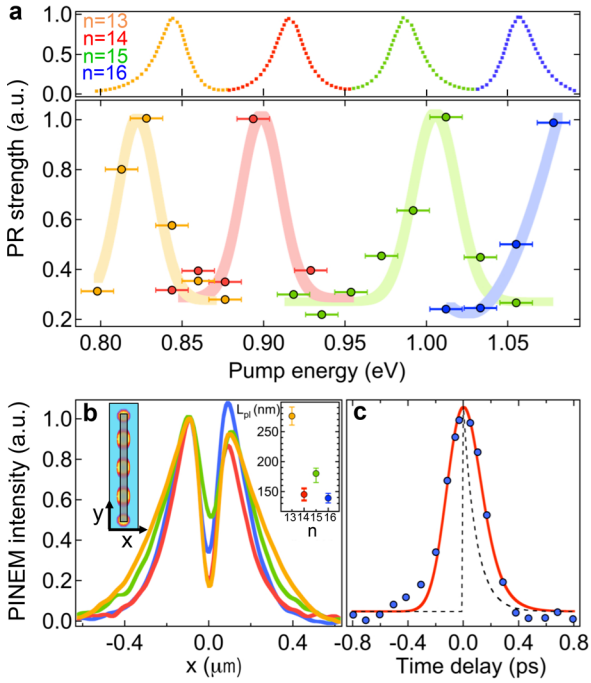

Figure 4. Energy, space, and time mapping of plasmons. (a) Normalized plasmon spectra for modes n = 13−16 (see color-coded labels) obtained upon scanning the laser energy between 0.8 (1550 nm) and 1.08 eV (1150 nm). Symbols are obtained with the integrated FT procedure explained in Figure 3. Thick lines are guides for the eye. Dashed curves on the top correspond to simulations of the normalized PR strengths for a nanowire of 7.8 μm length and 130 nm diameter. (b) Spatial profile of the photoexcited nanowire plasmonic field along the transversal x axis (left inset), obtained after integrating along the y wire axis for the different modes under consideration. Right inset: Spatial decay of the plasmonic field L_{pl} as a function of mode index n. (c) Temporal evolution of the photoexcited plasmonic field (blue circles), fitted with an exponential decay function (dashed black curve) convoluted with a Gaussian IRF (red curve).

figures for spatial profiles of all modes), highlighting the presence of n = 13−16 resonances. The optical excitation of both even and odd modes in the geometry of our experiment is due to the skew angle of the long wire relative to the electron beam direction.[9] The measured spectra are in good agreement with SRPINEM simulations based upon boundary-element-method calculations of the optical field (see Methods), except for an energy misalignment that could originate in imperfections of the NW. These defects result in a deviation from the ideal Fabry−Perot reflections calculated in a featureless wire, for which a more uniform mode spacing is predicted. In Figure 4b, we show the transversal spatial profile along the direction perpendicular to the nanowire axis; the plasmonic field is observed to decay exponentially with a characteristic length of 280 ± 20 nm for n = 13, roughly diminishing with the increasing order of the resonance, which is consistent with previous observations by spectral imaging[23] and also with an approximate transversal decay given by the plasmon wavelength divided by 2π.[14] The temporal evolution of the plasmonic field is depicted in Figure 4c, where we plot the intensity of the PINEM signal obtained with short electron bunches as a function of the time delay between laser and electron pulses. We obtain a plasmon lifetime of 90 ± 40 fs by fitting the measured temporal trace with a Gaussian instrument response function (IRF) of 250 ± 50 fs (see Figure S2 of ref 22) convoluted with a single-exponential decay. This method will be best suited for the investigation of very sharp long-lived (>1 ps) resonances, for instance in doped semiconductors.

We stress that this methodology is not limited by the energy broadening of the incident electron beam, in contrast to conventional inelastic scattering methods. In fact, the central frequency and the resolution necessary to image a specific mode are solely determined by the light excitation properties and not by the electron beam or spectrometer characteristics. This is an important advantage because light sources of high monochromaticity and controlled temporal profile are readily available at energies covering a wide spectral range, thus giving access to a broader parameter space compared with state-of-the-art electron optics. While in our current report we employ a fs infrared beam obtained via nonlinear wavelength conversion in an OPA, ultrahigh resolution spectroscopy experiments (even below 1 meV if one partially sacrifices time resolution) can be conceived using the intrinsic small line width of laser sources or incorporating spectral shaping techniques. Furthermore, our method can be applied to the investigation of arbitrarily low-energy modes, provided that they can be selectively excited by tunable light pulses. Clear candidates are phonons, which have been recently resolved in energy-filtered TEM[25] and can be photoexcited to manipulate the properties of quantum solids and nanostructures. By resolving the spectral, spatial, and temporal profiles of the light-induced phonon field in a nanostructure, one could simultaneously retrieve the dynamical coupling between the lattice and the electronic structure through line shape analysis, real-space observation of the coherent structural modes, and anharmonic decay in real time, yielding a valuable tool to visualize and control the physics of advanced nanostructured materials. Similarly, our method combined with the selective population of vibrational states in plasmonic nanoparticles, used as catalysis enhancers, could provide a unique high-resolution viewpoint in space, time, and energy on reaction trajectories.[31] Nanofabrication can also be used to modify selection rules and coupling strengths, making optically silent features accessible with our technique. In quantum solids, this method could be applied to a subset of collective excitations that couple to light, an example of which can be the transverse Josephson plasmons in layered superconductors.[32]

METHODS

Sample Preparation. Silver nanowires with a diameter of around 100 nm and lengths on the order of 10 μm (Sigma-Aldrich, 739421) were dispersed in ethanol through sonication for 30 min. Samples were then prepared by drop-casting a single drop of the resulting suspension on 50 nm thick Si_3N_4 support films (Ted Pella, 21509-10) and were air-dried for a couple of hours before examination in the ultrafast transmission electron microscope (UTEM, operated at 295 K and around 10^{-5} Pa).

Experimental Apparatus. A 300 kHz train of linearly polarized, 800 nm, 80 fs, 10 μJ light pulses was split to generate two beams. One beam was frequency tripled to deliver few-nJ ultraviolet pulses utilized to photoemit electrons from a truncated-cone LaB_6 cathode (15 μm diameter truncation plane, AP-Tech) in a modified JEOL JEM 2100 microscope operated at 200 kV,[29] as schematically shown in Figure 1a. The second 800 nm beam was used to seed an optical parametric amplifier (TOPAS HR, Light Conversion), producing signal

DOI: 10.1021/acsphotonics.7b01393
ACS Photonics 2018, 5, 759−764

beams between 1150 (1080 meV) and 1550 nm (800 meV), with energy per pulse in the 1−2 μJ range, depending on the wavelength. After passing through an optical delay line, the near-IR pulses were focused with a lens of 25 cm focal length inside the UTEM to a spot size of around 40 μm, such that uniform photoexcitation in the field-of-view of the photoelectron beam was obtained. The pump spot size was measured by a beam profiler (Spiricon, model SP620U), detecting a portion of the beam selected by a window and located at a distance from the lens corresponding to that of the specimen. The electron beam was perpendicular to the sample (i.e., to the thin film substrate), although the NWs could still be tilted with respect to it. For the PINEM experiments, a constant optical fluence of 5 mJ cm^{-2} at all wavelengths was used. Polarization of the pump pulses was set by using a broadband half-wave plate in the near-IR spectral regime. Energy-filtering of the electrons was performed by a postcolumn Gatan Quantum GIF electron energy-loss spectrometer. A 2048 × 2048 pixel CCD camera operated with a dispersion setting of 0.05 eV per channel was used to detect the filtered electrons. Imaging was performed by using an electron beam with ∼10^2 electrons per pulse and selecting a 4 eV window at the center of the ∼6 eV zero-loss peak obtained under these electron intensity conditions. Images of the wire in the presence of the pump pulse and before its arrival were obtained with 20 min integration and 5 min alternation to average over fluctuations of the electron beam intensity and sample position.

Image Processing. Images of the investigated NW at all wavelengths with and without the photoexcitation were spatially aligned using a 2D cross-correlation algorithm, after correcting for the different overall amount of counts caused by temporal fluctuations of electron beam intensity and instrumental conditions. Spikes above a fixed threshold value were removed, and single-pixel noise was median-filtered. Background was subtracted from every image after fitting its spatial distribution. Then, images of the photoinduced plasmonic fields were retrieved by taking the difference between the images recorded before and in coincidence with the photoexcitation. Spatial image calibration was performed by comparing the size of the nanowire with independent references.

Numerical Simulations. The interaction between swift electrons (velocity v, moving along z) and nearly monochromatic light (frequency ω, electric field E_z along z) in PINEM is quantified by the coupling integral $\beta = (e\gamma/\hbar\omega)\int \mathrm{d}z\, E_z(z)\, \mathrm{e}^{-i\omega z/v}$, where $\gamma = 1/\sqrt{1 - v^2/c^2}$.[33] The probability that the electron has gained or lost an energy $l\hbar\omega$ is $J_l^2(2|\beta|)$, so in particular, the depletion of the zero-loss peak ($l = 0$) is $1 - J_0^2(2|\beta|) \approx |\beta|^2$ for small β. We take this value as an estimate of the SRPINEM signal, calculated for each electron impact parameter relative to the wire, with the light electric field obtained via the boundary-element method[34] under external light illumination of a silver NW (130 nm diameter, 7.8 μm length, dielectric function from ref 35). The wire is taken to be oriented at 45° from the electron beam direction.

■ ASSOCIATED CONTENT

Supporting Information

The Supporting Information is available free of charge on the ACS Publications website at DOI: 10.1021/acsphotonics.7b01393.

Three supplementary figures, displaying the same information as Figure 3, but for the n = 14, 15, and 16 modes (PDF)

■ AUTHOR INFORMATION

Corresponding Author

*E-mail: fabrizio.carbone@epfl.ch.

ORCID

Enrico Pomarico: 0000-0001-5946-5310

Author Contributions

E.P., I.M., G.B., G.M.V., K.W. conducted the experiments; E.P. performed the data analysis; F.J.G.d.A. performed the simulations; F.C. conceived and designed the research; E.P., I.K., F.J.G.d.A., and F.C. wrote the article. All authors have read and approved the final manuscript.

Notes

The authors declare no competing financial interest.

■ ACKNOWLEDGMENTS

The LUMES laboratory acknowledges support from the NCCR MUST of the Swiss National Science Foundation. E.P. acknowledges financial support from the Swiss National Science Foundation through an Advanced Postdoc Mobility Grant (P300P2_158473). F. J. G. d. A. acknowledges financial support from the Spanish MINECO (MAT2014-59096-P and SEV2015-0522), AGAUR (2014 SGR 1400), Fundació Privada Cellex, and the Catalan CERCA program. The authors would like to thank A. Cavalleri, A. Howie, and D. Alexander for useful discussions.

■ REFERENCES

(1) Witczak-Krempa, W.; Chen, G.; Kim, Y. B.; Balents, L. Correlated Quantum Phenomena in the Strong Spin-Orbit Regime. *Annu. Rev. Condens. Matter Phys.* **2014**, *5*, 57−82.

(2) Ament, L. J. P.; van Veenendaal, M.; Devereaux, T. P.; Hill, J. P.; van den Brink, J. Resonant inelastic x-ray scattering studies of elementary excitations. *Rev. Mod. Phys.* **2011**, *83*, 705−67.

(3) Devereaux, T. P.; Hackl, R. Inelastic light scattering from correlated electrons. *Rev. Mod. Phys.* **2007**, *79*, 175−233.

(4) Nellist, P. D.; Pennycook, S. J. Subangstrom Resolution by Underfocused Incoherent Transmission Electron Microscopy. *Phys. Rev. Lett.* **1998**, *81*, 4156−59.

(5) Lazar, S.; Botton, G. A.; Zandbergen, H. W. Enhancement of resolution in core-loss and low-loss spectroscopy in a monochromated microscope. *Ultramicroscopy* **2006**, *106*, 1091−103.

(6) Mansart, B.; Lorenzana, J.; Mann, A.; Odeh, A.; Scarongella, M.; Chergui, M.; Carbone, F. Coupling of a high-energy excitation to superconducting quasiparticles in a cuprate from coherent charge fluctuation spectroscopy. *Proc. Natl. Acad. Sci. U. S. A.* **2013**, *110*, 4539−44.

(7) Rossi, F.; Kuhn, T. Theory of ultrafast phenomena in photoexcited semiconductors. *Rev. Mod. Phys.* **2002**, *74*, 895−950.

(8) Valley, D. T.; Ferry, V. E.; Flannigan, D. J. Imaging Intra- and Interparticle Acousto-plasmonic Vibrational Dynamics with Ultrafast Electron Microscopy. *Nano Lett.* **2016**, *16*, 7302−8.

(9) Piazza, L.; Lummen, T. T. A.; Quinónez, E.; Murooka, Y.; Reed, B. W.; Barwick, B.; Carbone, F. Simultaneous observation of the

DOI: 10.1021/acsphotonics.7b01393
ACS Photonics 2018, 5, 759−764

quantization and the interference pattern of a plasmonic near-field. *Nat. Commun.* **2015**, *6*, 6407.
(10) Li, J. J.; Chen, J.; Reis, D. A.; Fahy, S.; Merlin, R. Optical probing of ultrafast electronic decay in Bi and Sb with slow phonons. *Phys. Rev. Lett.* **2013**, *110*, 047401.
(11) Bosman, M.; Ye, E.; Tan, S. F.; Nijhuis, C. A.; Yang, J. K. W.; Marty, R.; Mlayah, A.; Arbouet, A.; Girard, C.; Han, M.-H. Surface Plasmon Damping Quantified with an Electron Nanoprobe. *Sci. Rep.* **2013**, *3*, 1312.
(12) Fausti, D.; Tobey, R. I.; Dean, N.; Kaiser, S.; Dienst, A.; Hoffmann, M. C.; Pyron, S.; Takayama, T.; Takagi, H.; Cavalleri, A. Light-induced superconductivity in a stripe-ordered cuprate. *Science* **2011**, *331*, 189−91.
(13) Burresi, M.; Kampfrath, T.; van Oosten, D.; Prangsma, J. C.; Song, B. S.; Noda, S.; Kuipers, L. Magnetic light-matter interactions in a photonic crystal nanocavity. *Phys. Rev. Lett.* **2010**, *105*, 123901.
(14) Basov, D. N.; Fogler, M. M.; Garcia de Abajo, F. J. Polaritons in van der Waals materials. *Science* **2016**, *354*, 1992.
(15) Barwick, B.; Flannigan, D. J.; Zewail, A. H. Photon-induced near-field electron microscopy. *Nature* **2009**, *462*, 902−906.
(16) Park, S. T.; Lin, M.; Zewail, A. H. Photon-induced near-field electron microscopy (PINEM): theoretical and experimental. *New J. Phys.* **2010**, *12*, 123028.
(17) Zewail, A. H. Four-Dimensional Electron Microscopy. *Science* **2010**, *328*, 187−93.
(18) Feist, A.; Echternkamp, K. E.; Schauss, J.; Yalunin, S. V.; Schafer, S.; Ropers, C. Quantum coherent optical phase modulation in an ultrafast transmission electron microscope. *Nature* **2015**, *521*, 200−3.
(19) Vanacore, G. M.; Fitzpatrick, A. W. P.; Zewail, A. H. Four-dimensional electron microscopy: Ultrafast imaging, diffraction and spectroscopy in materials science and biology. *Nano Today* **2016**, *11*, 228−49.
(20) Guzzinati, G.; Béché, A.; Lourenço-Martins, H.; Martin, J.; Kociak, M.; Verbeeck, J. Probing the symmetry of the potential of localized surface plasmon resonances with phase-shaped electron beams. *Nat. Commun.* **2017**, *8*, 14999.
(21) Park, S. T.; Yurtsever, A.; Baskin, J. S.; Zewail, A. H. Graphene-layered steps and their fields visualized by 4D electron microscopy. *Proc. Natl. Acad. Sci. U. S. A.* **2013**, *110*, 9277−82.
(22) Lummen, T. T. A.; Lamb, R. J.; Berruto, G.; LaGrange, T.; Dal Negro, L.; García de Abajo, F. J.; McGrouther, D.; Barwick, B.; Carbone, F. Imaging and controlling plasmonic interference fields at buried interfaces. *Nat. Commun.* **2016**, *7*, 13156.
(23) Rossouw, D.; Botton, G. A. Plasmonic Response of Bent Silver Nanowires for Nanophotonic Subwavelength Waveguiding. *Phys. Rev. Lett.* **2013**, *110*, 066801.
(24) Krivanek, O. L.; Lovejoy, T. C.; Dellby, N.; Aoki, T.; Carpenter, R. W.; Rez, P.; Soignard, E.; Zhu, J.; Batson, P. E.; Lagos, M. J.; Egerton, R. F.; Crozier, P. A. Vibrational spectroscopy in the electron microscope. *Nature* **2014**, *514*, 209−12.
(25) Lagos, M. J.; Trugler, A.; Hohenester, U.; Batson, P. E. Mapping vibrational surface and bulk modes in a single nanocube. *Nature* **2017**, *543*, 529−32.
(26) Anker, J. N.; Paige Hall, W.; Lyandres, O.; Shah, N. C.; Zhao, J.; van Duyne, P. Biosensing with plasmonic nanosensors. *Nat. Mater.* **2008**, *7*, 442−453.
(27) Grigorenko, A. N.; Polini, M.; Novoselov, K. S. Graphene plasmonics. *Nat. Photonics* **2012**, *6*, 749−58.
(28) García de Abajo, F. J. Optical excitations in electron microscopy. *Rev. Mod. Phys.* **2010**, *82*, 209−75.
(29) Piazza, L.; Masiel, D. J.; LaGrange, T.; Reed, B. W.; Barwick, B.; Carbone, F. Design and implementation of a fs-resolved transmission electron microscope based on thermionic gun technology. *Chem. Phys.* **2013**, *423*, 79−84.
(30) García de Abajo, F. J.; Kociak, M. Electron energy-gain spectroscopy. *New J. Phys.* **2008**, *10*, 073035.
(31) Linic, S.; Aslam, U.; Boerigter, C.; Morabito, M. Photochemical transformations on plasmonic metal nanoparticles. *Nat. Mater.* **2015**, *14* (6), 567−76.
(32) Dulic, D.; Pimenov, A.; van der Marel, D.; Broun, D. M.; Kamal, S.; Hardy, W. N.; Tsvetkov, A. A.; Sutjaha, I. M.; Liang, R.; Menovsky, A. A.; Loidl, A.; Saxena, S. S. Observation of the transverse optical plasmon in $SmLa_{0.8}Sr_{0.2}CuO_{4-\delta}$. *Phys. Rev. Lett.* **2001**, *86*, 4144−7.
(33) García de Abajo, F. J.; Barwick, B.; Carbone, F. Electron diffraction by plasmon waves. *Phys. Rev. B: Condens. Matter Mater. Phys.* **2016**, *94*, 041404.
(34) García de Abajo, F. J.; Howie, A. Retarded field calculation of electron energy loss in inhomogeneous dielectrics. *Phys. Rev. B: Condens. Matter Mater. Phys.* **2002**, *65*, 115418.
(35) Johnson, P. B.; Christy, R. W. Optical Constants of the Noble Metals. *Phys. Rev. B* **1972**, *6*, 4370−9.

DOI: 10.1021/acsphotonics.7b01393
ACS Photonics 2018, 5, 759−764